Multiple superconducting phases driven by pressure in the topological insulator $GeSb_4Te_7$

W. Zhou [1,*] B. Li,[2] Y. Shen,[3] J. J. Feng,[4] C. Q. Xu,[5] H. T. Guo,[1] Z. He,[1] B. Qian,[1,†] Ziming Zhu,[3] and Xiaofeng Xu [6,‡]

[1]*School of Electronic and Information Engineering, Changshu Institute of Technology, Changshu 215500, China*

[2]*Information Physics Research Center, Nanjing University of Posts and Telecommunications, Nanjing 210023, China*

[3]*Key Laboratory of Low-Dimensional Quantum Structures and Quantum Control of Ministry of Education, Department of Physics and Synergetic Innovation Center for Quantum Effects and Applications, Hunan Normal University, Changsha 410081, China*

[4]*Center for High Pressure Science and Technology Advanced Research, Shanghai 201203, China*

[5]*School of Physical Science and Technology, Ningbo University, Ningbo 315211, China*

[6]*Department of Applied Physics, Zhejiang University of Technology, Hangzhou 310023, China*

(Received 5 June 2023; revised 19 October 2023; accepted 19 October 2023; published 2 November 2023)

Tuning superconductivity in topological materials by means of chemical substitution, electrostatic gating, or pressure is thought to be an effective route towards realizing topological superconductivity with their inherent Majorana fermions, the manipulation of which may form the basis for future topological quantum computing. It has recently been established that the pseudo-binary chalcogenides $(ACh)_m(Pn_2Ch_3)_n$ (A = Ge, Mn, Pb, etc.; Pn = Sb or Bi; Ch = Te, Se) may host novel topological quantum states such as the quantum anomalous Hall effect and topological axion states. Here we map out the phase diagram of one member in this series, the topological insulator candidate $GeSb_4Te_7$ up to pressures of ∼35 GPa, through a combination of electrical resistance measurements, Raman spectroscopy, as well as first-principles calculations. Three distinct superconducting phases emerge under the pressure above ∼11, ∼17, and ∼31 GPa, which are accompanied by concomitant structural transitions, evidenced from the changes in the Raman modes. The first-principles calculations validate the existence of a topological insulating state at ambient pressure and predict two possible structural transitions at 10 and 17 GPa, in agreement with the experimental observations. Overall, our results establish the $GeSb_4Te_7$ family of materials as a fertile arena for further exploring various topological phenomena, including topological phase transitions and putative topological superconductivity.

DOI: 10.1103/PhysRevB.108.184504

I. INTRODUCTION

Since the first theoretical proposals of two-dimensional (2D) and three-dimensional (3D) topological insulators (TIs), the material realizations of nontrivial electronic band topology with unconventional surface states and peculiar electromagnetic responses have become one of the most fascinating fields in solid-state physics [1–4]. Subsequently, time-reversal-symmetric, nonsymmorphic topological insulators; mirror Chern insulators; Dirac, Weyl, and nodal-line semimetals; as well as higher-fold degenerate fermions and high-order TIs have all been put forward theoretically and been verified experimentally [5–10]. The success achieved in the past decade has been further expedited by recently introduced theories of topological quantum chemistry and symmetry-based indicators (SIs) that have, in particular, facilitated high-throughput searches for topological phases of matter [8,9,11,12]. Although over 50% of all known materials exhibit symmetry-indicated nontrivial topology [13], only a very limited proportion of them become superconductors at low temperatures, either at ambient pressure or under hydrostatic pressure. This hinders the search for intrinsic topological superconductors in stoichiometric compounds, thereby presenting challenges in exploiting Majorana fermions for topological quantum computing.

In a large number of currently known topological materials, the layered binary chalcogenides Pn_2Ch_3 (Pn = Bi, Sb; Ch = Te, Se) were among the first validated TIs, both theoretically and experimentally [1,4]. These Bi_2Te_3-type compounds have tetradymite-like layered structures comprised of Te-Bi-Te-Bi-Te quintuple layers (5L, QLs) that are stacked by van der Waals forces along the c axis [Fig. 1(a)] [14]. This weak van der Waals force facilitates the chemical doping or intercalation. For example, the MnTe bilayer can readily intercalate the QLs, forming the Te-Bi-Te-Mn-Te-Bi-Te septuple layers (7L, SLs) [Fig. 1(b)]. With these QLs and SLs as the building blocks, new van der Waals compounds $(ACh)_m(Pn_2Ch_3)_n$ (A = Ge, Mn, Pb, etc.; Pn = Sb or Bi; Ch = Te, Se) can be synthesized [15–21]. Taking $MnBi_2Te_4$ ($m = 1$, $n = 1$) as an example, the structure is constructed by the stacking of SLs [Fig. 1(b)], whereas in $MnBi_4Te_7$ ($m = 1$, $n = 2$), it consists of alternating stacking of QLs and SLs along the c axis, forming naturally grown superlattices [Fig. 1(c)]. Interestingly, most members in this family were found to be 3D TIs [4,17,18,22,23], thereby providing a tunable platform to observe unusual topological phenomena.

*wei.zhou@cslg.edu.cn
†njqb@cslg.edu.cn
‡xuxiaofeng@zjut.edu.cn

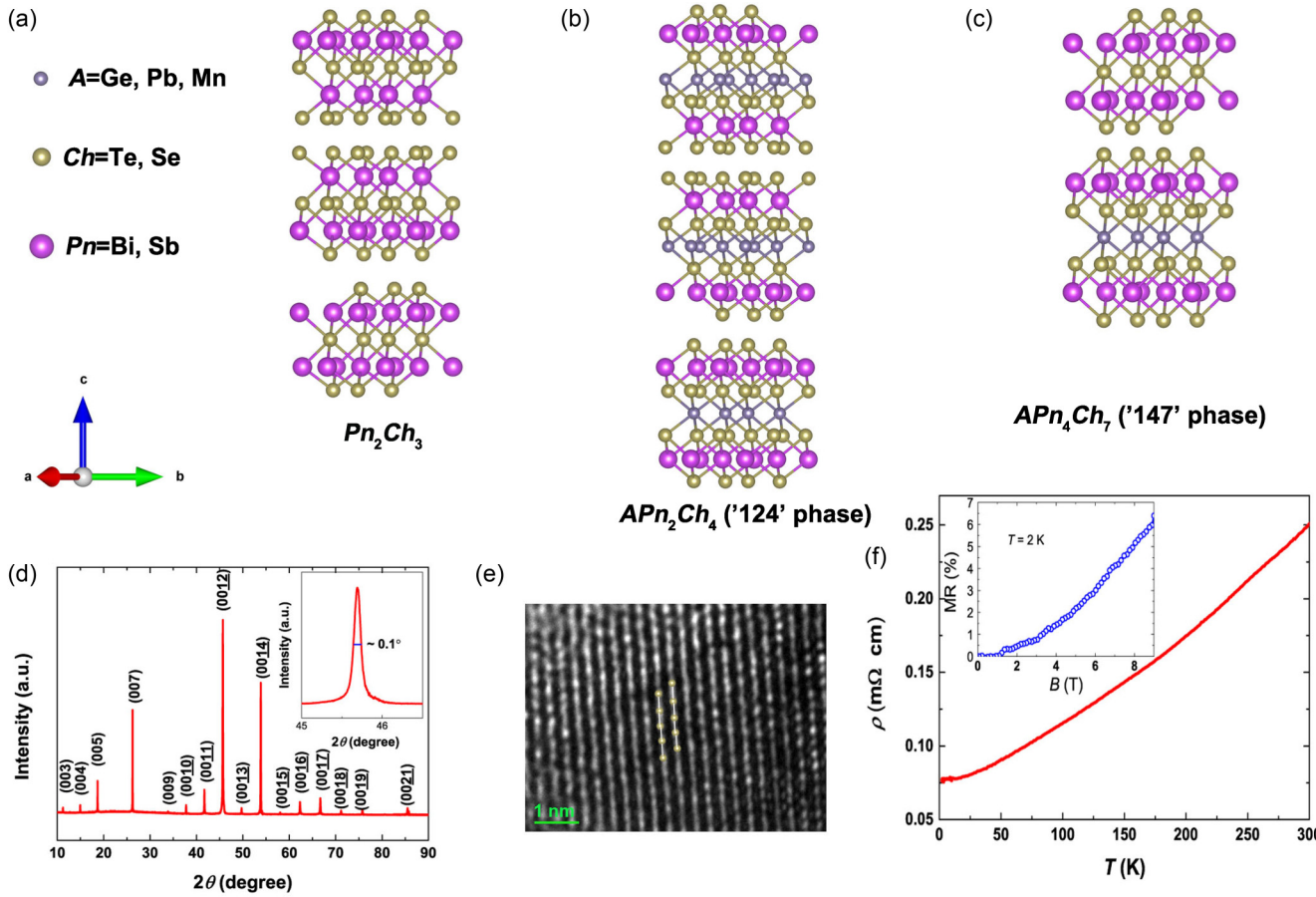

FIG. 1. (a)–(c) Crystal structures of Pn_2Ch_3, APn_2Ch_4 ("124" phase), and APn_4Ch_7 ("147" phase) at ambient pressure. The structures are drawn using the software VESTA [24]. (d) The ambient XRD pattern of a $GeSb_4Te_7$ single crystal. Inset is an enlarged view of the (00$\underline{12}$) peak with a FWHM of 0.1°. (e) TEM image of the crystal. (f) Temperature dependence of the resistivity at ambient pressure. Inset shows the magnetoresistance (MR) measured at $T = 2$ K at ambient pressure.

Previously, much effort has been devoted to realizing superconductivity in the $(ACh)_m(Pn_2Ch_3)_n$ compounds, and pressure has been demonstrated to be an important tool for tuning structural phase transitions and superconductivity thereof [25–30]. For example, in Sb_2Te_3, four superconducting phases were revealed under pressures up to 32 GPa that are correlated with four distinct structures [26]. In $SnSb_2Te_4$, superconductivity was found to be gradually enhanced with pressure up to 33 GPa [28]. In both crystalline $GeSb_2Te_4$ and amorphous $GeSb_2Te_4$, two superconducting phases were observed for $P < 40$ GPa and the maximum superconducting transition temperature was observed at 20–30 GPa [29,30].

Notably, the magnetic members in families such as $MnBi_2Te_4$ and $MnBi_4Te_7$, have attracted more interest recently, with the desire to observe the quantum anomalous Hall (QAH) effect and axion insulator state with quantized topological magnetoelectric effect [15–18,31–34]. Following the first observation of the QAH effect in Cr-doped $(Bi,Sb)_2Te_3$ TI thin films [35], the focus has shifted towards intrinsic magnetic topological materials that are thought to provide a cleaner platform for studying emergent magnetic topological states. Indeed, QAH was observed in $MnBi_2Te_4$ thin flakes with an odd number of SLs [16]. On the other hand, pressure has also been employed to tune the ground states of these magnetic topological materials. Specifically, it was reported that pressure induces several structural transitions in $MnBi_2Te_4$ and $MnBi_4Te_7$, which change their topological properties simultaneously [36]. However, no superconductivity was observed in both systems up to ∼50 GPa [36]. More recently, pressure-induced superconductivity was observed in the Mn-based "147" antiferromagnet $MnSb_4Te_7$ with a maximum T_c of 2.2 K at 50 GPa [37]. A natural question arises as to the possible role played by the magnetic fluctuations in its superconductivity since the element Mn is generally magnetic. In particular, whether the magnetic fluctuations are energetically favorable or adverse for the formation of superconductivity in this topological family is unclear.

With all these in mind, we performed a high-pressure study of the nonmagnetic counterpart $GeSb_4Te_7$ that is isostructural to $MnSb_4Te_7$. We reveal three distinct superconducting phases under pressure above 11, 17, and 31 GPa, which are concomitant with three structural transitions, different from the pressure phase diagrams reported in Sb_2Te_3, $SnSb_2Te_4$, $GeSb_2Te_4$, etc. [25–30]. Importantly, the superconducting transition temperature T_c in pressurized $GeSb_4Te_7$ is a factor of 4 higher than that in its pressurized magnetic homologue $MnSb_4Te_7$. This significantly enhanced T_c suggests that the magnetic fluctuations may have adverse effects on the Cooper pair formation in this 147 phase of pseudo-binary systems,

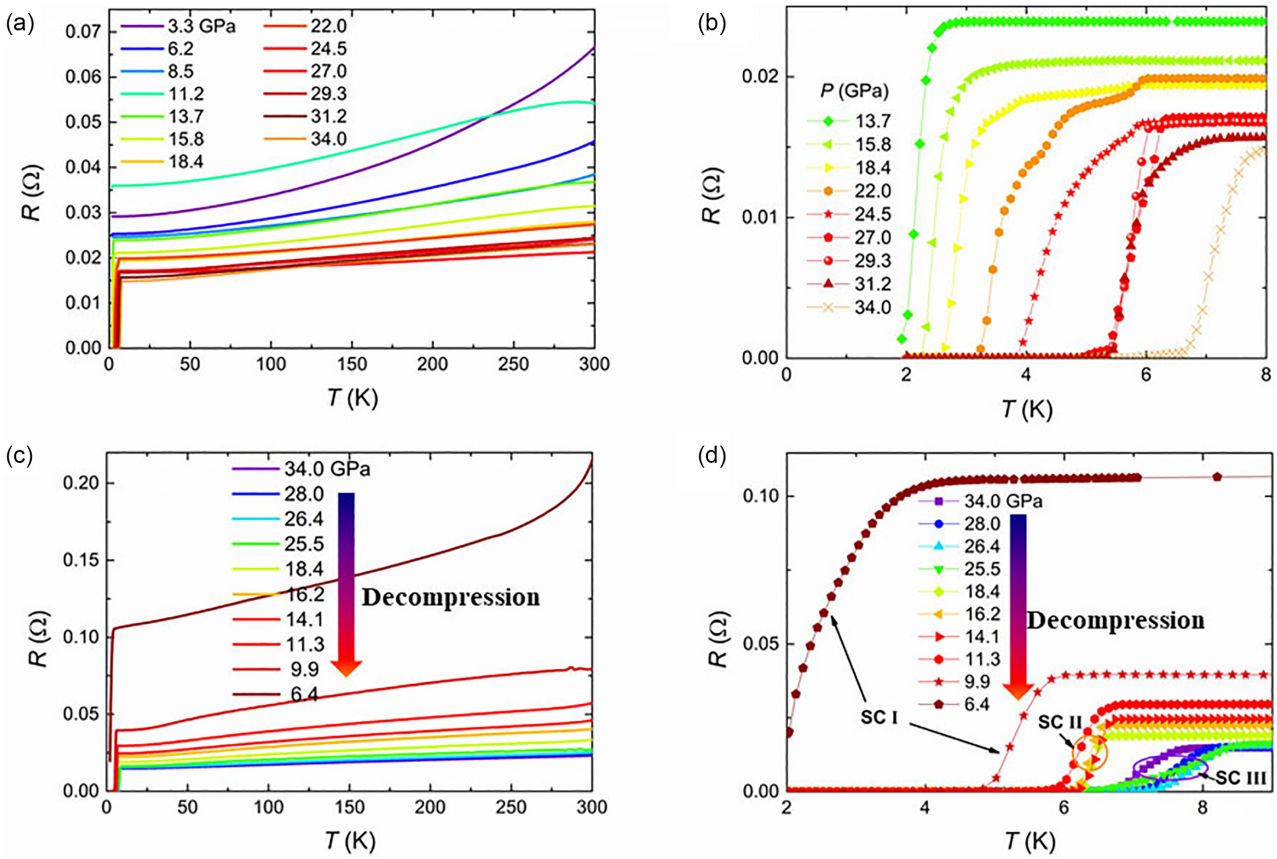

FIG. 2. (a) Temperature dependence of the resistance $R(T)$ for different pressures measured during the compression process. (b) An enlarged view of (a) in the low-temperature region. (c) $R(T)$ curves for different pressures measured during the decompression process. (d) A low-temperature enlargement of panel (c).

although both $GeSb_4Te_7$ and $MnSb_4Te_7$ show unambiguous topological features.

II. EXPERIMENT

Single crystals of $GeSb_4Te_7$ were grown by the flux method reported in Ref. [38]. Single crystal and powder x-ray diffraction (XRD) measurements were performed at room temperature using a diffractometer with Cu $K\alpha$ radiation. The actual composition of the single crystals was characterized by an energy dispersive x-ray spectroscopy (EDXS) analyzer equipped on a scanning electronic microscope and a transmission electron microscope (TEM). The EDXS results confirm that the atomic ratio for Ge:Sb:Te is very close to 1:4:7. The specific heat data were measured on a physical property measurement system (PPMS-9, Quantum Design). The transport data under pressure were acquired from measurements in a diamond-anvil cell with NaCl as the pressure transmitting medium. High-pressure Raman spectroscopy data were collected by a Renishaw inVia Raman system with a laser wavelength of 532 nm.

The electronic band structure calculations were performed using the full-potential linearized augmented plane wave method implemented in the WIEN2K code [39]. We employed a tight-binding dependent package WANNIERTOOLS for topological properties investigations [40]. The iterative Green's function was used for obtaining the surface-state spectrum. We used the in-house developed crystal structure prediction package CRYSTREE to search for the stable structures of $GeSb_4Te_7$ under pressure [41]. We then employed the QUANTUM ESPRESSO package [42] with Perdew-Burke-Ernzerhof exchange-correlation functional to compute the enthalpies of the predicted structures under various pressures. The cutoff values for charge density and the wave function were set to be 600 and 60 Ry, respectively.

III. RESULTS

Figure 1(d) shows the single crystal XRD pattern for one $GeSb_4Te_7$ crystal under ambient conditions. Only the reflections from the $(00l)$ planes are observed, indicating that the crystallographic c axis is normal to the sample surface. The sharp peaks demonstrate the high quality of the single crystal, with a FWHM of the $(00\underline{12})$ peak of about 0.1°, exemplified in the inset of Fig. 1(d). As shown in Fig. S1 of the Supplemental Material, all peaks of the powder XRD from the pulverized crystals can be well indexed by the trigonal $P\bar{3}m1$ (No. 164) space group [43]. The calculated lattice parameters are $a = 4.23$ Å and $c = 23.82$ Å, in excellent agreement with the published results [44]. The TEM image further demonstrates the high quality of the single crystal, as illustrated in Fig. 1(e). The temperature-dependent resistivity shows typical metallic behavior from room temperature all the way down to 2 K [Fig. 1(f)], with no superconductivity observed in this

temperature range. The residual resistivity ratio ($R_{300\,\mathrm{K}}/R_{2\,\mathrm{K}}$) is rather small (~3.3), indicating significant electron scattering. The inset of Fig. 1(f) shows the magnetoresistance (MR) measured at 2 K. In comparison with many TIs, the MR value is relatively small, which may also be related to significant electron scattering. The heat capacity characterization of the sample shows no evident anomaly below 200 K (Fig. S2 of Ref. [43]). The fit based on the electron and phonon contributions $C(T) = \gamma_n T + \beta T^3 + \eta T^5$ yields a Sommerfeld coefficient $\gamma_n = 2.43$ mJ/mol K^2, and a Debye temperature $\Theta_D = 187.5$ K. This small Sommerfeld coefficient implies weak electron correlations in this material.

The $R(T)$ profiles measured under various pressures upon compression are shown in Fig. 2. With increasing pressure, the $R(T)$ curves are gradually suppressed up to 8.5 GPa, above which the $R(T)$ curve shows a sudden increase (see 11.2 GPa data). Simultaneously, in the low-T region, the $R(T)$ curve ($P = 11.2$ GPa) shows a small resistance drop, indicating incipient superconductivity. As P further increases, the superconducting transition becomes prominent and zero resistance can be observed. Meanwhile, the normal-state $R(T)$ curve shifts downwards again. As seen in Fig. 2(b), the superconducting transition gradually moves towards higher temperatures as P changes from 13.7 to 24.5 GPa. However, for $P > 24.5$ GPa, the superconducting transition barely changes with increasing P. Above 31.0 GPa, a large enhancement of T_c can be seen, reaching a maximum value of 8 K at 34 GPa, the highest pressure measured in this study. In parallel, Figs. 2(c) and 2(d) show the resistance during the pressure decompression process, measured with the same electrical contacts as in the pressure compression course. With decreasing pressure, the above-mentioned main features in the $R(T)$ curves and P-dependent superconducting transitions can be overall reproduced, with the exception that superconductivity can now be seen at much lower pressures. Specifically, at the lowest pressure of ~6.4 GPa measured upon decompression, the superconducting transition can still be observed below ~3.8 K, whereas when compressing, the critical pressure for observing superconductivity is approximately ~11.2 GPa.

The pressure dependences of the $R(T)$ curves, the superconducting transition temperatures, as well as the room-temperature resistances during compression are summarized in the phase diagram in Fig. 3. As noted, the emergence of superconductivity around 11 GPa is accompanied by a sudden increase of the resistance at 300 K, implying a possible phase transition around ~11 GPa. With increasing pressure, T_c is gradually enhanced at a rate of ~0.21 K/GPa while the resistance at room temperature is smoothly suppressed. We designate this superconducting phase as SC I. As the pressure increases to 18.4 GPa, the resistance displays a small drop around 6 K initially, followed by a major decrease at 4 K. This two-step drop of resistance suggests two possible superconducting transitions and was also seen under 22 GPa. For $P > 24.5$ GPa, only one SC transition can be observed and T_c barely changes with pressure, displaying a $T_c(P)$ plateau with a T_c value of ~6 K. A similar weak pressure dependence of T_c has also been observed in the pressure phase diagrams of Bi_2Se_3 and Sb_2Te_3, which was shown to be closely related to the charge-carrier density [25,26]. We denote this phase as SC II. When $P > 31$ GPa, T_c shows a large increase, and $R_{300\,\mathrm{K}}$ starts to decrease again. These changes suggest a possible phase transition taking place around 31 GPa and we therefore label the superconducting phase for $P > 31$ GPa as SC III. The room-temperature resistance as a function of pressure is displayed in Fig. 3(b). For the phase diagram for the decompression process, see Fig. S3 in Ref. [43].

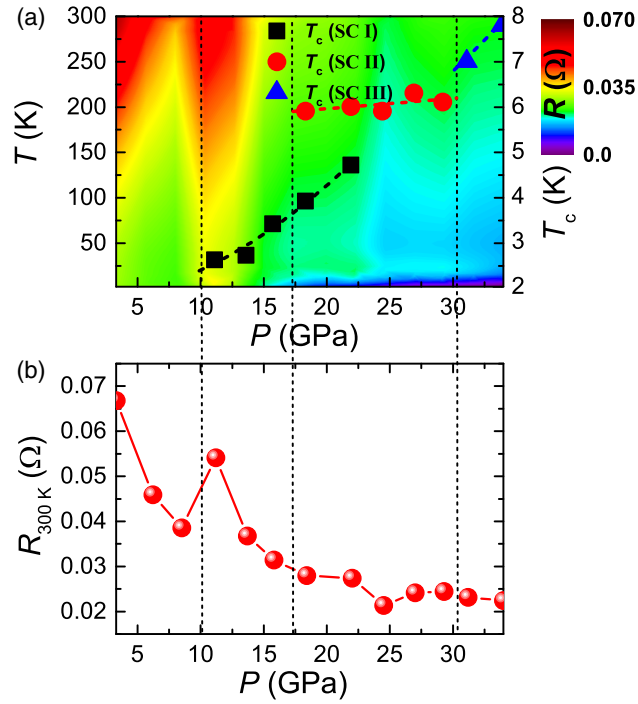

FIG. 3. (a) Pressure-dependent phase diagram based on the data measured during the compression process. The right vertical coordinate denotes the onset superconducting transition temperature T_c. (b) Pressure dependence of the resistance at 300 K.

The distinction between the SC II and SC III phases is not only manifested in their different pressure dependence of T_c, but is also reflected in their temperature-dependent upper critical field ($\mu_0 H_{c2}$) behaviors as displayed in Fig. 4(c). The $\mu_0 H_{c2}$ values are extracted from the superconducting transitions under different fields shown in Figs. 4(a) and 4(b), based on the commonly used 90% criterion where the resistance drops to 90% of the normal-state value. It is worth noting that choosing a different criterion (e.g., 50% criterion or zero resistance) does not qualitatively change the overall behavior. In Fig. 4(c), the fittings based on the Ginzburg-Landau formula $\mu_0 H_{c2}(T) = \mu_0 H_{c2}(0)(1-t^2)/(1+t^2)$, where $t = T/T_c$, lead to $\mu_0 H_{c2}(0) = 3.1$ T for 18.4 GPa (SC II) and $\mu_0 H_{c2}(0) = 1.6$ T for 34.0 GPa (SC III). Generally, for the same superconducting phase, a higher superconducting transition temperature often results in a higher $\mu_0 H_{c2}(0)$. However, here the superconductivity at 34 GPa (SC III) has a higher T_c value but with a lower $\mu_0 H_{c2}(0)$, in contrast to the ~6 K superconductivity of SC II, and therefore one can conclude that these two superconductivity phases are different in nature.

Pressure-dependent Raman spectra were measured and are displayed in Fig. 4(d). At $P \sim 3.3$ GPa, two distinct Raman modes at 106 cm^{-1} (E_g) and 121 cm^{-1} (A_{1g}) are observed [45]. As P increases, the Raman peaks move towards higher

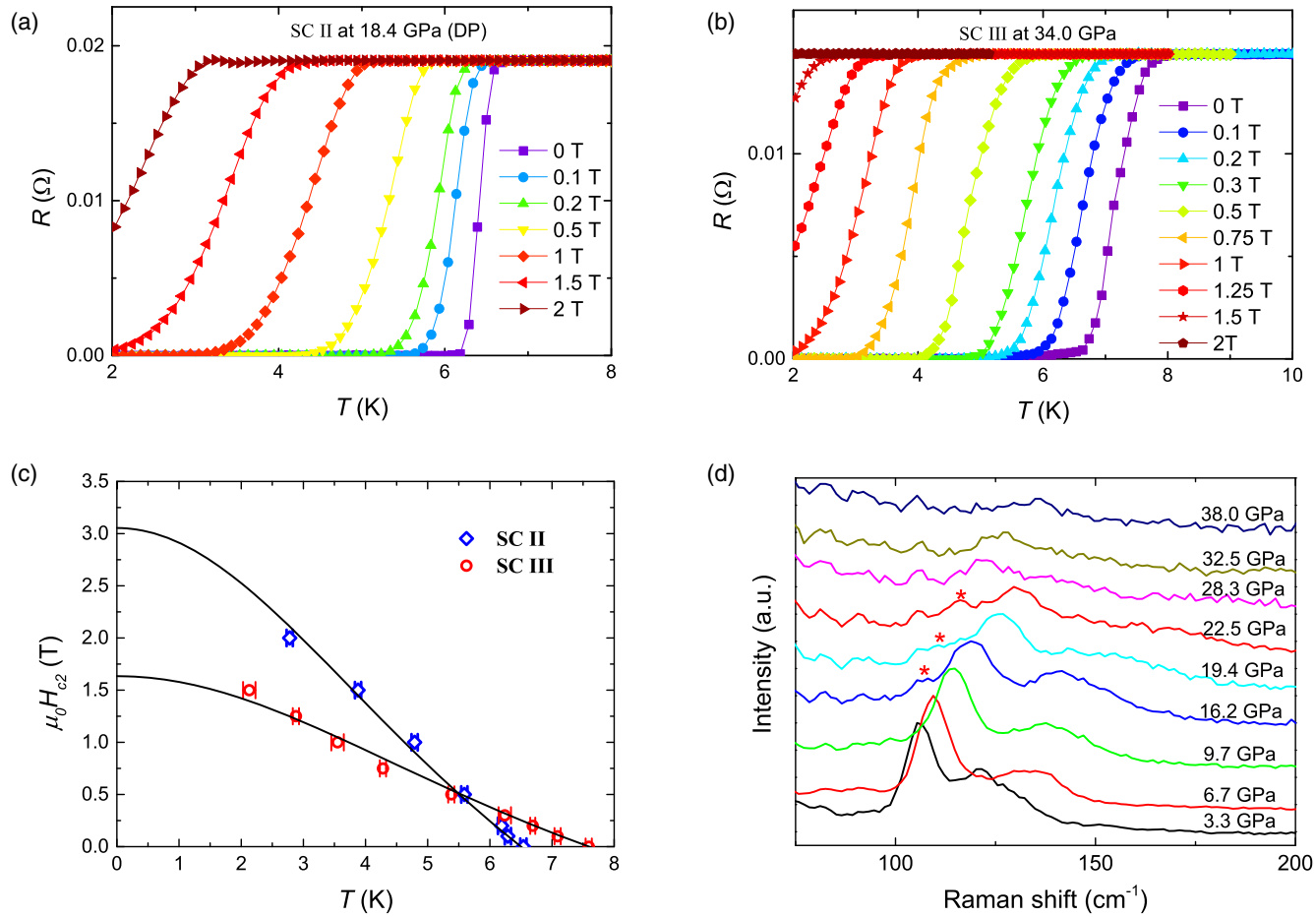

FIG. 4. (a) and (b) The superconducting transitions measured under different magnetic fields. (c) Temperature dependence of the upper critical field $\mu_0 H_{c2}$. The solid lines are fits based on the Ginzburg-Landau formula, that is, $\mu_0 H_{c2}(T) = \mu_0 H_{c2}(0)(1-t^2)/(1+t^2)$, where $t = T/T_c$, yielding $\mu_0 H_{c2}(0) = 3.1$ T for SC II and $\mu_0 H_{c2}(0) = 1.6$ T for SC III. (d) Raman spectra measured under different pressures.

wave numbers. When P is increased from 9.7 to 16.2 GPa, a new vibration mode labeled by a red star emerges, suggestive of a structural phase transition. This structural phase transition is also consistent with the transition revealed from the transport measurements discussed above. When P is increased from 22.5 to 28.3, the main E_g mode disappears, implying the occurrence of another structural phase transition, which agrees with the transition from the SC I to SC II. For $P >$ 30 GPa, the Raman peaks become very weak, which probably results from the pressure-induced amorphization or another structural transition.

The electronic band structure of the pristine phase ($P\bar{3}m1$) at ambient pressure is shown in Fig. 5(b). A small energy gap of ~0.07 eV opens up around the Fermi level, suggesting a semiconducting ground state. The metallic behaviors revealed in the resistivity measurements indicate that the as-grown samples are naturally doped due to small off-stoichiometry or native defects. As seen, the valence bands are predominantly contributed by Te atoms, whereas the conduction bands are dominated by Sb orbitals. We also studied the topological properties of the $P\bar{3}m1$ phase under the tight-binding framework. The Z_2 topological indices (ν_0; $\nu_1\nu_2\nu_3$) can be estimated through the calculation of Wannier charge centers in six time-reversal invariant planes (i.e., $k_x = 0, \pi, k_y = 0, \pi$, and $k_z = 0, \pi$ planes). The resultant topological index for the $P\bar{3}m1$ phase is (1; 001), which indicates that the $P\bar{3}m1$ phase is a strong topological insulator. Figure 5(c) illustrated the surface-state spectrum of the (0 0 1) surface of $GeSb_4Te_7$, with evident Dirac surface states crossing the Fermi level in the bulk band gap, indicating its topological insulator properties.

To illuminate the nature of the transitions revealed in the transport and Raman spectroscopy measurements, we made an attempt to predict the crystal structure under pressure using the first-principles calculations, as shown in Fig. 5(d). Here we calculated the enthalpy of different phases with increasing pressure and the most stable phase has the lowest enthalpy in general. Our results show that $GeSb_4Te_7$ maintains the ambient structure up to $P \sim 10$ GPa, above which the $C2/m$ phase becomes the most stable. This phase is energetically favorable until a pressure of ~17 GPa where $GeSb_4Te_7$ undergoes a structural transition to the Cm phase. This structural prediction may be overall consistent with the first two structural transitions seen in the experiments. However, our calculations cannot resolve the third transition around 30 GPa, which merits further studies in the future. The band structures of the high-pressure $C2/m$ and Cm phases are also calculated (see Fig. S4 in Ref. [43]). The nontrivial topological characteristics are manifested in these pressure-induced new phases, evidenced from nonzero Z_2 invariants. Specifically, the cal-

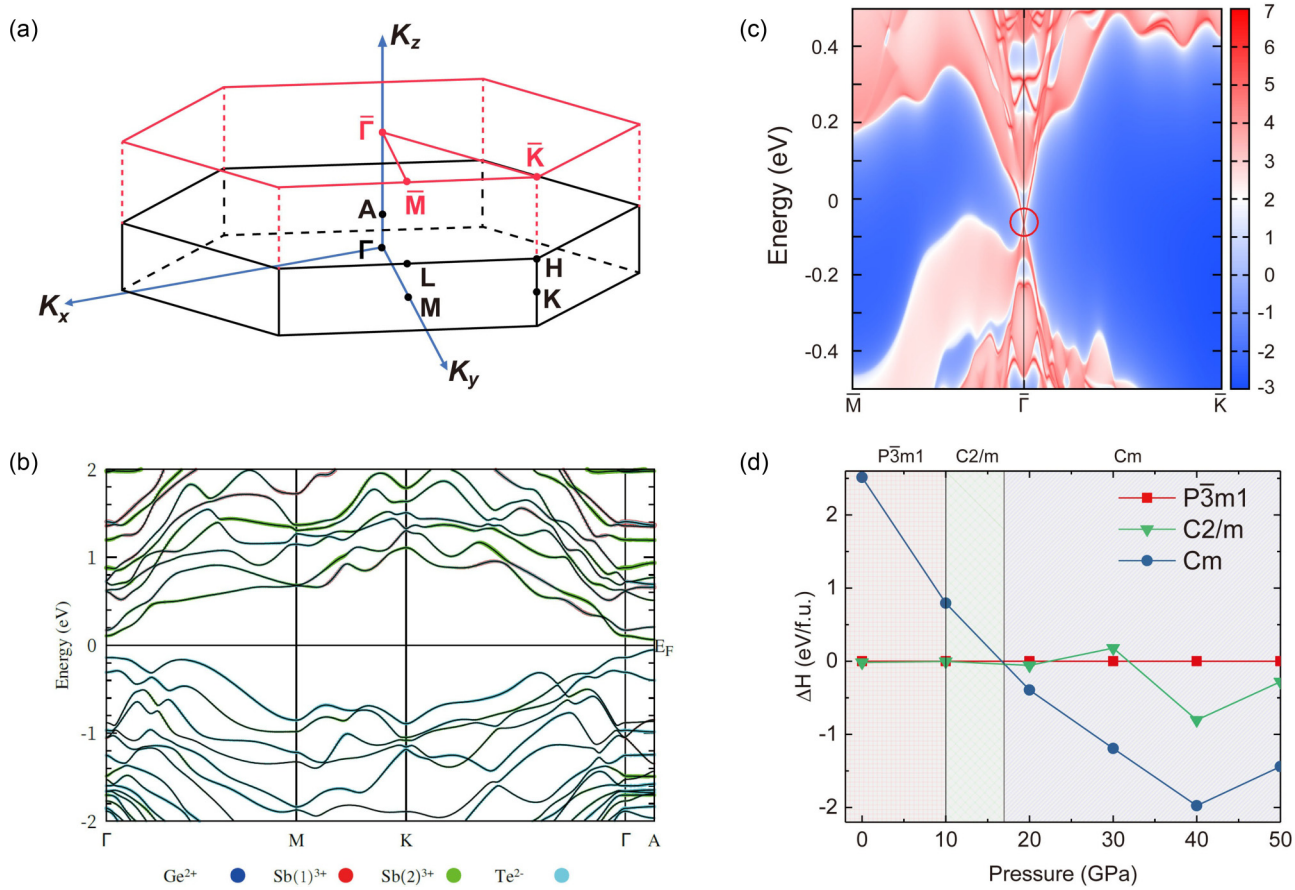

FIG. 5. (a) Bulk and (001)-surface Brillouin zone of $GeSb_4Te_7$ for the $P\bar{3}m1$ phase. (b) The electronic band structure of the $P\bar{3}m1$ phase colored by elemental characters at ambient pressure. (c) Surface state for the (001) surface along high-symmetry directions. (d) Calculated enthalpies of different phases as a function of pressure. The enthalpy of the $P\bar{3}m1$ phase at the corresponding pressure is taken as the reference enthalpy, i.e., $\Delta H = H(\text{phase}) - H(P\bar{3}m1)$.

culation of the $C2/m$ phase at 10 GPa exhibits a Z_2 index of (1, 010), demonstrating that it is a strong topological insulator, whereas for the Cm phase at 20 GPa, the calculated Z_2 index is (0, 111), indicating it is a weak topological material.

IV. DISCUSSION AND CONCLUSION

Having established the phase diagram of the title compound under pressure, it is important to understand its topological properties and superconductivity by comparing to those in the same family of $(ACh)_m(Pn_2Ch_3)_n$. Topological surface states have been unambiguously demonstrated in spin-resolved angle-resolved photoelectron spectroscopy (ARPES) measurements on $Ge(Bi_{1-x}Sb_x)_4Te_7$ with x ranging from $x = 0$ to $x = 0.25$ [22]. With increasing Sb content, the Dirac point on the surface moves towards the Fermi level, changing from n- to p-type carriers at $x = 0.15$. Albeit with no direct ARPES measurement on the end member $GeSb_4Te_7$ thus far, it is conceivable that it also harbors Dirac cones on its surface, as suggested from our first-principles calculations above. Recently, versatile topological phases have been reported in the 147 magnetic $MnSb_4Te_7$ whose topological properties can be tuned either by carrier doping or by magnetic field, through the change of magnetic configurations via the latter [23]. On the other hand, extensive efforts have been made to tune the superconductivity in this class of materials by pressure but most of them are unsuccessful. For example, applying pressure on $MnBi_2Te_4$ and $MnBi_4Te_7$ only induces several structural transitions and the concomitant changes of topological properties, with no superconductivity being observed up to 50 GPa [36]. In magnetic $MnSb_4Te_7$ with weaker magnetic interactions, evidenced from its lower magnetic transition temperatures compared with $MnBi_2Te_4$ and $MnBi_4Te_7$, superconductivity was observed when $P >$ 30 GPa, reaching a maximum T_c of 2 K at 50 GPa [37]. This does seem to suggest that magnetic fluctuations play an adverse role in the superconductivity, at least in this class of materials. This argument gets further support from the observations of superconductivity in the nonmagnetic counterpart $GeSb_4Te_7$ uncovered in this study, as well as the reported pressure-induced superconductivity in $GeSb_2Te_4$ ($T_c = 6$ K at $P = 20$ GPa) [29,30], which are both nonmagnetic.

From the structural point of view, the 147 phase can be viewed as the combination of Pn_2Ch_3 and the 124 phase (see Fig. 1). Naively, given the weak van der Waals force between the quintuple layer and the septuple layer, one may expect that the pressure effect for the 147 phase would be a combination of that for the Pn_2Ch_3 phase and the 124 phase. However, the pressure effect on $GeSb_4Te_7$, as revealed in this study, is quite different from both that of Sb_2Te_3 and the 124 $GeSb_2Te_4$

[26,29,30]. In Sb_2Te_3, for example, superconductivity was observed under pressures as low as 4.0 GPa, and four superconducting phases have been identified up to 32 GPa [26]. In $GeSb_2Te_4$ (here we only consider the crystalline $GeSb_2Te_4$ phase [29]), superconductivity was induced at ∼10 GPa and two superconducting phases were suggested with a maximum T_c (∼8 K) around 20–30 GPa [29]. For $GeSb_4Te_7$, the lowest pressure for observing superconductivity is also around 10 GPa, which is comparable to that for $GeSb_2Te_4$ but much higher than that of Sb_2Te_3. In the pressure range of 10–30 GPa, the phase diagrams for $GeSb_2Te_4$ and $GeSb_4Te_7$ are quite similar. However, a definite third superconducting phase (SC III) is observed in $GeSb_4Te_7$ for $P > 30$ GPa, which appears to be absent in $GeSb_2Te_4$.

In summary, we have performed a systematic high-pressure study of the topological insulator $GeSb_4Te_7$ which reveals multiple phase transitions upon compression. Three superconducting phases were uncovered in our high-pressure study up to 35 GPa, where the corresponding changes in their Raman spectroscopy suggest the presence of structural transitions under pressure. However, first-principles calculations only reproduced the first two transitions and therefore point to the need for future studies to reveal the nature of all these structural transitions. This work not only provides further impetus for studying novel topological phenomena in these pseudo-binary chalcogenides $(ACh)_m(Pn_2Ch_3)_n$, but also calls for future investigations into the interplay between the topological states and the emergent superconductivity in the pressurized phases of this class of materials.

ACKNOWLEDGMENTS

The authors thank Michael Smidman, Xiangang Wan, and Dong Qian for helpful discussions. This work was sponsored by the National Natural Science Foundation of China (Grants No. 11704047, No. U1832147, and No. U1932217). X.X. acknowledges the financial support from National Natural Science Foundation of China (Grants No. 12274369 and No. 11974061).

W.Z. and B.L. contributed equally to this work.

[1] M. Z. Hasan and C. L. Kane, *Colloquium*: Topological insulators, Rev. Mod. Phys. **82**, 3045 (2010).

[2] X. L. Qi and S. C. Zhang, Topological insulators and superconductors, Rev. Mod. Phys. **83**, 1057 (2011).

[3] B. Yan and S. C. Zhang, Topological materials, Rep. Prog. Phys. **75**, 096501 (2012).

[4] Y. Ando, Topological insulator materials, J. Phys. Soc. Jpn. **82**, 102001 (2013).

[5] B. Yan and C. Felser, Topological materials: Weyl semimetals, Annu. Rev. Condens. Matter Phys. **8**, 337 (2017).

[6] B. A. Bernevig, C. Felser, and H. Beidenkopf, Progress and prospects in magnetic topological materials, Nature (London) **603**, 41 (2022).

[7] F. Tang, H. C. Po, A. Vishwanath, and X. Wan, Comprehensive search for topological materials using symmetry indicators, Nature (London) **566**, 486 (2019).

[8] Y. Xu, L. Elcoro, Z. D. Song, B. J. Wieder, M. G. Vergniory, N. Regnault, Y. Chen, C. Felser, and B. A. Bernevig, High-throughput calculations of magnetic topological materials, Nature (London) **586**, 702 (2020).

[9] H. C. Po, A. Vishwanath, and H. Watanabe, Symmetry-based indicators of band topology in the 230 space groups, Nat. Commun. **8**, 50 (2017).

[10] T. H. Hsieh, H. Lin, J. Liu, W. Duan, A. Bansil, and Liang Fu, Topological crystalline insulators in the SnTe material class, Nat. Commun. **3**, 982 (2012).

[11] M. G. Vergniory, L. Elcoro, C. Felser, N. Regnault, B. A. Bernevig, and Z. Wang, A complete catalogue of high-quality topological materials, Nature (London) **566**, 480 (2019).

[12] B. Bradlyn, L. Elcoro, J. Cano, M. G. Vergniory, Z. Wang, C. Felser, M. I. Aroyo, and B. A. Bernevig, Topological quantum chemistry, Nature (London) **547**, 298 (2017).

[13] M. G. Vergniory, B. J. Wieder, L. Elcoro, S. S. P. Parkin, C. Felser, B. A. Bernevig, and N. Regnault, All topological bands of all nonmagnetic stoichiometric materials, Science **376**, eabg9094 (2022).

[14] S. V. Eremeev, G. Landolt, T. V. Menshchikova, B. Slomski, Y. M. Koroteev, Z. S. Aliev, M. B. Babanly, J. Henk, A. Ernst, L. Patthey, A. Eich, A. A. Khajetoorians, J. Hagemeister, O. Pietzsch, J. Wiebe, R. Wiesendanger, P. M. Echenique, S. S. Tsirkin, I. R. Amiraslanov, J. H. Dil and E. V. Chulkov, Atom-specific spin mapping and buried topological states in a homologous series of topological insulators, Nat. Commun. **3**, 635 (2012).

[15] J. Li, Y. Li, S. Du, Z. Wang, B.-L. Gu, S.-C. Zhang, K. He, W. Duan, and Y. Xu, Intrinsic magnetic topological insulators in van der Waals layered $MnBi_2Te_4$-family materials, Sci. Adv. **5**, eaaw5685 (2019).

[16] Y. Deng, Y. Yu, M. Z. Shi, Z. Guo, Z. Xu, J. Wang, X. H. Chen, and Y. Zhang, Quantum anomalous Hall effect in intrinsic magnetic topological insulator $MnBi_2Te_4$, Science **367**, 895 (2020).

[17] M. M. Otrokov, I. I. Klimovskikh, H. Bentmann, D. Estyunin, A. Zeugner, Z. S. Aliev, S. Gass, A. U. B. Wolter, A. V. Koroleva, A. M. Shikin, M. Blanco-Rey, M. Hoffmann, I. P. Rusinov, A. Y. Vyazovskaya, S. V. Eremeev, Y. M. Koroteev, V. M. Kuznetsov, F. Freyse, J. Sanchez-Barriga, I. R. Amiraslanov *et al.*, Prediction and observation of an antiferromagnetic topological insulator, Nature (London) **576**, 416 (2019).

[18] C. Hu, K. N. Gordon, P. Liu, J. Liu, X. Zhou, P. Hao, D. Narayan, E. Emmanouilidou, H. Sun, Y. Liu, H. Brawer, A. P. Ramirez, L. Ding, H. Cao, Q. Liu, D. Dessau, and N. Ni, A van der Waals antiferromagnetic topological insulator with weak interlayer magnetic coupling, Nat. Commun. **11**, 97 (2020).

[19] S. Chowdhury, K. F. Garrity, and F. Tavazza, Prediction of Weyl semimetal and antiferromagnetic topological insulator phases in Bi_2MnSe_4, npj Comput. Mater. **5**, 33 (2019).

[20] J. L. F. Da Silva, A. Walsh, and H. Lee, Insights into the structure of the stable and metastable $(GeTe)_m(Sb_2Te_3)_n$ compounds, Phys. Rev. B **78**, 224111 (2008).

[21] J.-W. Park, S. H. Eom, H. Lee, J. L. F. Da Silva, Y.-S. Kang, T.-Y. Lee, and Y. H. Khang, Optical properties of pseudobinary

GeTe, $Ge_2Sb_2Te_5$, $GeSb_2Te_4$, $GeSb_4Te_7$, and Sb_2Te_3 from ellipsometry and density functional theory, Phys. Rev. B **80**, 115209 (2009).

[22] S. Muff, F. von Rohr, G. Landolt, B. Slomski, A. Schilling, R. J. Cava, J. Osterwalder, and J. H. Dil, Separating the bulk and surface *n*- to *p*-type transition in the topological insulator $GeBi_{4-x}Sb_xTe_7$, Phys. Rev. B **88**, 035407 (2013).

[23] S. Huan, S. Zhang, Z. Jiang, H. Su, H. Wang, X. Zhang, Y. Yang, Z. Liu, X. Wang, N. Yu, Z. Zou, D. Shen, J. Liu, and Y. Guo, Multiple magnetic topological phases in bulk van der Waals crystal $MnSb_4Te_7$, Phys. Rev. Lett. **126**, 246601 (2021).

[24] K. Momma and F. Izumi, VESTA 3 for three-dimensional visualization of crystal, volumetric and morphology data, J. Appl. Crystallogr. **44**, 1272 (2011).

[25] P. P. Kong, J. L. Zhang, S. J. Zhang, J. Zhu, Q. Q. Liu, R. C. Yu, Z. Fang, C. Q. Jin, W. G. Yang, X. H. Yu, J. L. Zhu, and Y. S. Zhao, Superconductivity of the topological insulator Bi_2Se_3 at high pressure, J. Phys.: Condens. Matter **25**, 362204 (2013).

[26] J. Zhu, J. L. Zhang, P. P. Kong, S. J. Zhang, X. H. Yu, J. L. Zhu, Q. Q. Liu, X. Li, R. C. Yu, R. Ahuja, W. G. Yang, G. Y. Shen, H. K. Mao, H. M. Weng, X. Dai, Z. Fang, Y. S. Zhao, and C. Q. Jin, Superconductivity in topological insulator Sb_2Te_3 induced by pressure, Sci. Rep. **3**, 2016 (2013).

[27] R. Matsumoto, Z. Hou, M. Nagao, S. Adachi, H. Hara, H. Tanaka, K. Nakamura, R. Murakami, S. Yamamoto, H. Takeya, T. Irifune, K. Terakura, and Y. Takano, Data-driven exploration of new pressure-induced superconductivity in $PbBi_2Te_4$, Sci. Technol. Adv. Mater. **19**, 909 (2018).

[28] P. Song, R. Matsumoto, Z. Hou, S. Adachi, H. Hara, Y. Saito, P. B. Castro, H. Takeya, and Y. Takano, Pressure-induced superconductivity in $SnSb_2Te_4$, J. Phys.: Condens. Matter **32**, 235901 (2020).

[29] E. Greenberg, B. Hen, S. Layek, I. Pozin, R. Friedman, V. Shelukhin, Y. Rosenberg, M. Karpovski, M. P. Pasternak, E. Sterer, Y. Dagan, G. K. Rozenberg, and A. Palevski, Superconductivity in multiple phases of compressed $GeSb_2Te_4$, Phys. Rev. B **95**, 064514 (2017).

[30] B. Hen, S. Layek, M. Goldstein, V. Shelukhin, M. Shulman, M. Karpovski, E. Greenberg, E. Sterer, Y. Dagan, G. K. Rozenberg, and A. Palevski, Superconductor-insulator transition in fcc $GeSb_2Te_4$ at elevated pressures, Phys. Rev. B **97**, 024513 (2018).

[31] S. H. Lee, Y. Zhu, Y. Wang, L. Miao, T. Pillsbury, H. Yi, S. Kempinger, J. Hu, C. A. Heikes, P. Quarterman, W. Ratcliff, J. A. Borchers, H. Zhang, X. Ke, D. Graf, N. Alem, C.-Z. Chang, N. Samarth, and Z. Mao, Spin scattering and noncollinear spin structure-induced intrinsic anomalous Hall effect in antiferromagnetic topological insulator $MnBi_2Te_4$, Phys. Rev. Res. **1**, 012011(R) (2019).

[32] H. Li, S.-Y. Gao, S.-F. Duan, Y.-F. Xu, K.-J. Zhu, S.-J. Tian, J.-C. Gao, W.-H. Fan, Z.-C. Rao, J.-R. Huang, J.-J. Li, D.-Y. Yan, Z.-T. Liu, W.-L. Liu, Y.-B. Huang, Y.-L. Li, Y. Liu, G.-B. Zhang, P. Zhang, T. Kondo *et al.*, Dirac surface states in intrinsic magnetic topological insulators $EuSn_2As_2$ and $MnBi_{2n}Te_{3n+1}$, Phys. Rev. X **9**, 041039 (2019).

[33] J. Li, C. Wang, Z. Zhang, B.-L. Gu, W. Duan, and Y. Xu, Magnetically controllable topological quantum phase transitions in the antiferromagnetic topological insulator $MnBi_2Te_4$, Phys. Rev. B **100**, 121103(R) (2019).

[34] R. C. Vidal, H. Bentmann, T. R. F. Peixoto, A. Zeugner, S. Moser, C. H. Min, S. Schatz, K. Kißner, M.Ünzelmann, C. I. Fornari, H. B. Vasili, M. Valvidares, K. Sakamoto, D. Mondal, J. Fujii, I. Vobornik, S. Jung, C. Cacho, T. K. Kim, R. J. Koch *et al.*, Surface states and Rashba-type spin polarization in antiferromagnetic $MnBi_2Te_4$(0001), Phys. Rev. B **100**, 121104(R) (2019).

[35] C.-Z. Chang, J. Zhang, X. Feng, J. Shen, Z. Zhang, M. Guo, K. Li, Y. Ou, P. Wei, L. Wang, Z.-Q. Ji, Y. Feng, S. Ji, X. Chen, J. Jia, X. Dai, Z. Fang, S.-c. Zhang, K. He, Y. Wang *et al.*, Experimental observation of the quantum anomalous Hall effect in a magnetic topological insulator, Science **340**, 167 (2013).

[36] C. Pei, Y. Xia, J. Wu, Y. Zhao, L. Gao, T. Ying, B. Gao, N. Li, W. Yang, D. Zhang, H. Gou, Y. Chen, H. Hosono, G. Li, and Y. Qi, Pressure-induced topological and structural phase transitions in an antiferromagnetic topological insulator, Chin. Phys. Lett. **37**, 066401 (2020).

[37] C. Pei, M. Xi, Q. Wang, W. Shi, J. Wu, L. Gao, Y. Zhao, S. Tian, W. Cao, C. Li, M. Zhang, S. Zhu, Y. Chen, H. Lei, and Y. Qi, Pressure-induced superconductivity in magnetic topological insulator candidate $MnSb_4Te_7$, Phys. Rev. Mater. **6**, L101801 (2022).

[38] F. von Rohr, A. Schilling, and R. J. Cava, Single-crystal growth and thermoelectric properties of $Ge(Bi, Sb)_4Te_7$, J. Phys.: Condens. Matter **25**, 075804 (2013).

[39] P. Blaha, K. Schwarz, and P. Sorantin, Full-potential, linearized augmented plane wave programs for crystalline systems, Comput. Phys. Commun. **59**, 399 (1990).

[40] Q. Wu, S. Zhang, H. F. Song, M. Troyer, and A. A. Soluyanov, WannierTools: An open-source software package for novel topological materials, Comput. Phys. Commun. **224**, 405 (2018).

[41] S. Wu, B. Li, Z. Chen, Y. Hou, Y. Bai, X. Hao, Y. Yang, S. Liu, J. Cheng, and Z. Shi, Phase transitions and superconductivity in ternary hydride Li_2SiH_6 at high pressures, J. Appl. Phys. **131**, 065901 (2022).

[42] P. Giannozzi, S. Baroni, N. Bonini, M. Calandra, M. Calandra, R. Car, C. Cavazzoni, D. Ceresoli, G. L. Chiarotti, M. Cococcioni, and I. Dabo, QUANTUM ESPRESSO: A modular and open-source software project for quantum simulations of materials, J. Phys.: Condens. Matter **21**, 395502 (2009).

[43] See Supplemental Material at http://link.aps.org/supplemental/10.1103/PhysRevB.108.184504 for more sample characterizations, the phase diagram in the decompression process, as well as the band structure of the high-pressure phases.

[44] I. I. Petrov, R. M. Imamov, and Z. G. Pinsker, Electron-diffraction determination of the structures of $Ge_2Sb_2Te_5$ and $GeSb_4Te_7$, Sov. Phys. Crystallogr. **13**, 339 (1968).

[45] P. Mal, G. Bera, G. R. Turpu, S. K. Srivastava, A. Gangan, B. Chakraborty, B. Das, and P. Das, Vibrational spectra of $Pb_2Bi_2Te_3$, $PbBi_2Te_4$, and $PbBi_4Te_7$ topological insulators: Temperature-dependent Raman and theoretical insights from DFT simulations, Phys. Chem. Chem. Phys. **21**, 15030 (2019).